

Freezing out of a low-energy bulk spin exciton in SmB_6

K. Akintola,¹ A. Pal,¹ S. R. Dunsiger,¹ A. C. Y. Fang,¹ M. Potma,^{1,2}

S. R. Saha,³ X. F. Wang,³ J. Paglione,^{3,4} and J. E. Sonier,^{1,4}

¹*Department of Physics, Simon Fraser University, Burnaby, British Columbia V5A 1S6, Canada*

²*Kwantlen Polytechnic University, Richmond, British Columbia V6X 3X7, Canada*

³*Center for Nanophysics and Advanced Materials, Department of Physics,
University of Maryland, College Park, Maryland 20742, USA*

⁴*Canadian Institute for Advanced Research, Toronto, Ontario M5G 1Z8, Canada*

(Dated: March 9, 2024)

The Kondo insulator SmB_6 is purported to develop into a robust topological insulator at low temperature. Yet there are several puzzling and unexplained physical properties of the insulating bulk. It has been proposed that bulk spin excitons may be the source of these anomalies and may also adversely affect the topologically-protected metallic surface states. Here, we report muon spin rotation (μSR) measurements of SmB_6 that show thermally-activated behavior for the temperature dependences of the transverse-field (TF) relaxation rate below 20 K and muon (μ^+) Knight shift below 5-6 K. Our data are consistent with the freezing out of a bulk low-energy (~ 1 meV) spin exciton concurrent with the appearance of metallic surface conductivity. Furthermore, our results support the idea that spin excitons play some role in the anomalous low-temperature bulk properties of SmB_6 .

INTRODUCTION

Due to a combination of spin-orbit coupling and time reversal symmetry, a topological insulator (TI) supports protected metallic edge and surface states in two-dimensional (2-D) and three-dimensional (3-D) systems, respectively.¹ The ideal 3-D TI has a truly insulating bulk gap, as this restricts applications of the transport properties to the topologically-protected surface, where the electron spin is uniquely locked to the charge momentum. Yet true bulk insulating behavior is not realized in established TIs due to bulk impurity conduction.² The homogeneous intermediate-valence compound SmB_6 is a strong candidate for a 3-D TI with a robust bulk insulating gap.³ In contrast to a conventional band insulator, the insulating gap in SmB_6 is created via Kondo hybridization of localized $\text{Sm-}4f$ and itinerant $\text{Sm-}5d$ electrons, with the Fermi level residing in the hybridization gap.

Experimental evidence for SmB_6 being a TI is provided by transport measurements that have demonstrated predominant surface electrical conduction below 5-7 K,⁴⁻⁶ and the detection of in-gap surface states by angle-resolved photoemission spectroscopy (ARPES).⁷⁻¹¹ However, recent high-resolution ARPES results suggest that the surface conductivity is not associated with topological surface states.¹² Moreover, at low T there is a sizable metallic-like linear- T specific heat of bulk origin,¹³ and significant bulk ac-conduction.¹⁴ Quantum oscillations are observed in the magnetization of SmB_6 as expected for 2-D metallic surface states,¹⁵ but subsequent measurements suggest the origin is a bulk 3-D Fermi surface.¹⁶ These findings have raised the possibility of charge-neutral fermions in the insulating bulk.¹⁷⁻¹⁹

The Sm ions in SmB_6 rapidly fluctuate between non-magnetic Sm^{2+} ($4f^6$) and magnetic Sm^{3+} ($4f^5 5d^1$) electronic configurations, resulting in an average intermediate valence that varies with temperature.^{20,21} Interestingly, SmB_6 exhibits magnetic fluctuations below 20-

25 K where the Kondo gap is fully formed, as observed by muon spin relaxation/rotation (μSR).^{22,23} This was first presumed²² to be due to the bulk magnetic in-gap states detected by nuclear magnetic resonance (NMR) below 20 K,²⁴ and later specifically speculated to be due to bulk spin excitonic excitations.²⁵ Spin excitons in SmB_6 are induced by residual dynamic AFM exchange interactions between the hybridized quasiparticles and are a precursor to an AFM instability.^{26,27} A 14 meV bulk collective mode observed within the hybridization gap by inelastic neutron scattering (INS) has been interpreted as a spin exciton.^{28,29} Bulk spin excitons are expected to adversely affect the protected topological order by causing spin-flip scattering of the surface states.³⁰ There is some indirect evidence for this from recent angle-integrated photoemission³¹ and planar tunneling³² spectroscopy studies.

Since an implanted μ^+ does not create a spin-exciton excitation, μSR is only sensitive to thermally-activated spin excitons. Consequently, the 14 meV bulk spin exciton observed by INS should not be detectable by μSR below 20-25 K. An additional lower energy ($\lesssim 1$ meV) spin-exciton branch has recently been predicted and suggested to contribute to bulk quantum oscillations and cause the anomalous upturn in the specific heat at low T .³³ On the other hand, the low- T specific heat is enhanced by Gd impurities³⁴ and drastically reduced in isotopically enriched SmB_6 ,³⁵ suggesting magnetic impurities play some role but spin excitons do not. Nevertheless, decoupling of the surface states from a ~ 4 meV bulk spin exciton has been argued to explain the rapid increase in the surface conductance below 5-6 K and subsequent saturation below 4 K.³² While the reduction in energy from 14 meV to 4 meV is assumed to be due to a diminished Kondo temperature at the surface,³⁰ a distinct low-energy bulk spin exciton is another possibility.

Here we report high TF- μSR measurements of the

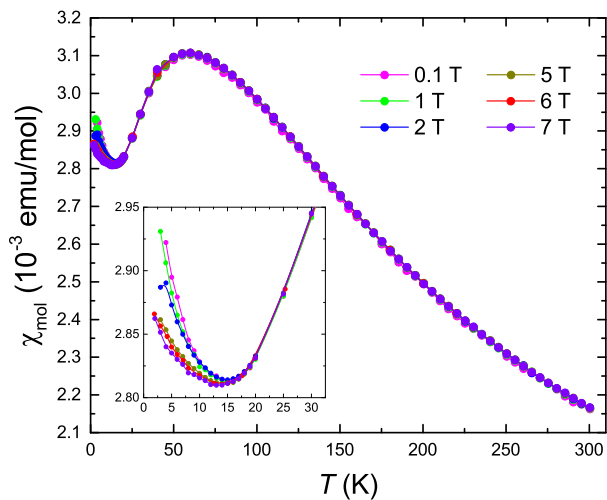


FIG. 1. Temperature dependence of the bulk magnetic susceptibility for fields applied parallel to the c -axis. The inset is a blow up of the low- T data.

μ^+ -Knight shift in Al-flux grown SmB_6 single crystals that provide evidence for a bulk spin exciton of energy much lower than 14 meV. Our data suggest that the occurrence of a resistivity plateau below $T \sim 4$ K is associated with the freezing out of an ~ 1 meV spin exciton, such that metallic surface states emerge when spin exciton scattering becomes negligible.

RESULTS

Figure 1 shows the temperature dependence of the bulk magnetic susceptibility χ_{mol} at different magnetic fields \mathbf{H} applied parallel to the c -axis. At high temperature χ_{mol} exhibits Curie-Weiss behavior indicative of paramagnetic Sm ions. Opening of the hybridization gap below 110 K gives rise to the broad maximum, followed by a field-dependent upturn below $T \sim 17$ K that masks the expected low- T van-Vleck saturation. The upturn has previously been attributed to impurities.^{36,37}

In the absence of spontaneous magnetic order, the applied field polarizes the conduction electrons and induces spin polarization of the localized Sm-4*f* magnetic moments. The local field \mathbf{B}_μ sensed by the μ^+ is the vector sum of the dipolar field \mathbf{B}_{dip} from the Sm-4*f* magnetic moments and a contact hyperfine field \mathbf{B}_c . At high T where SmB_6 behaves as a poor metal, the muon's positive charge is screened by a cloud of conduction electrons. The screening electron cloud acquires a finite spin density due to the Ruderman-Kittel-Kasuya-Yosida (RKKY) interaction with the spin-polarized Sm-4*f* moments, and by direct contact generates a hyperfine field at the μ^+ site. This is expected to vanish with the development of a bulk insulating gap at lower T . In an insulating state \mathbf{B}_c may instead originate from direct overlap of the μ^+ with the wavefunction of localized magnetic electrons, or from bonding of the μ^+ to an ion that is covalently bonded to a local atomic magnetic moment.³⁸

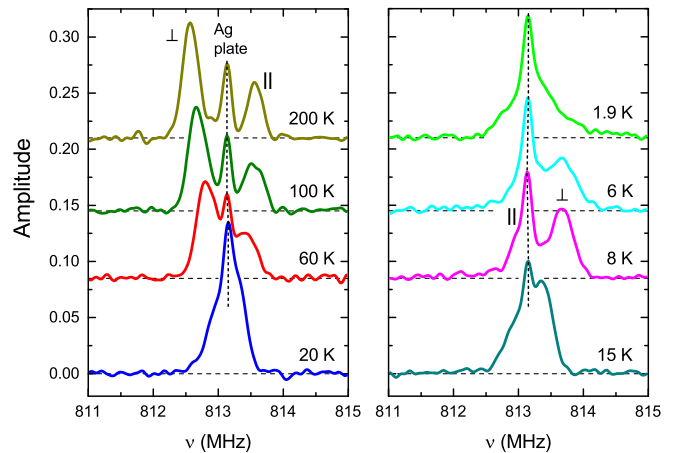


FIG. 2. Fourier transforms of representative TF- μ SR spectra at $H = 6$ T applied parallel to the c -axis. The frequency ν is equivalent to $(\gamma_\mu/2\pi)B_\mu$.

Figure 2 shows Fourier transforms of TF- μ SR time spectra recorded on SmB_6 at $H = 6$ T. Due to the apodization necessary to remove ringing artifacts caused by the short muon time window ($\sim 10 \mu\text{s}$) and noise caused by fewer counts at later times (due to the short muon lifetime), the Fourier transforms are a broadened visual approximation of the internal magnetic field distribution. Consequently, analysis of the TF- μ SR signals were done in the time domain. At $T = 200$ K there are three well separated peaks in the Fourier transform. The central peak arises from muons stopping in the Ag backing plate. The left and right peaks have an amplitude ratio of 2:1, and are consistent with the μ^+ stopping at the midpoint of the horizontal or vertical edges of the cubic Sm-ion sublattice. This is in agreement with the identified μ^+ site in CeB_6 .³⁹ Moreover, we have verified the μ^+ site assignment by TF- μ SR measurements with \mathbf{H} applied 45° with respect to the c -axis (see Fig. S3).

In a field applied parallel to the c -axis, the μ^+ site is magnetically inequivalent on the horizontal and vertical edges of the cubic Sm sublattice. The dipole field generated by polarization of the Sm-4*f* moments along the c direction is equivalent and antiparallel to \mathbf{H} at the (\perp) sites $(\frac{1}{2}, 0, 0)$ and $(0, \frac{1}{2}, 0)$, and different in magnitude and parallel to \mathbf{H} at the (\parallel) site $(0, 0, \frac{1}{2})$ (see Fig. 3a inset). Consequently, the TF- μ SR time spectra were fit to an asymmetry function with a two-component sample contribution (see Fig. S4)

$$A(t) = A_s \left[\frac{2}{3} e^{-\Delta_\perp^2 t^2} \cos(2\pi\nu_\perp t + \phi) \right. \quad (1)$$

$$\left. + \frac{1}{3} e^{-\Delta_\parallel^2 t^2} \cos(2\pi\nu_\parallel t + \phi) \right] \quad (2)$$

$$+ A_{\text{Ag}} e^{-\Delta_{\text{Ag}}^2 t^2} \cos(2\pi\nu_{\text{Ag}} t + \phi). \quad (3)$$

Here A_s and A_{Ag} denote the initial asymmetries of the sample and Ag backing plate contributions, respectively.

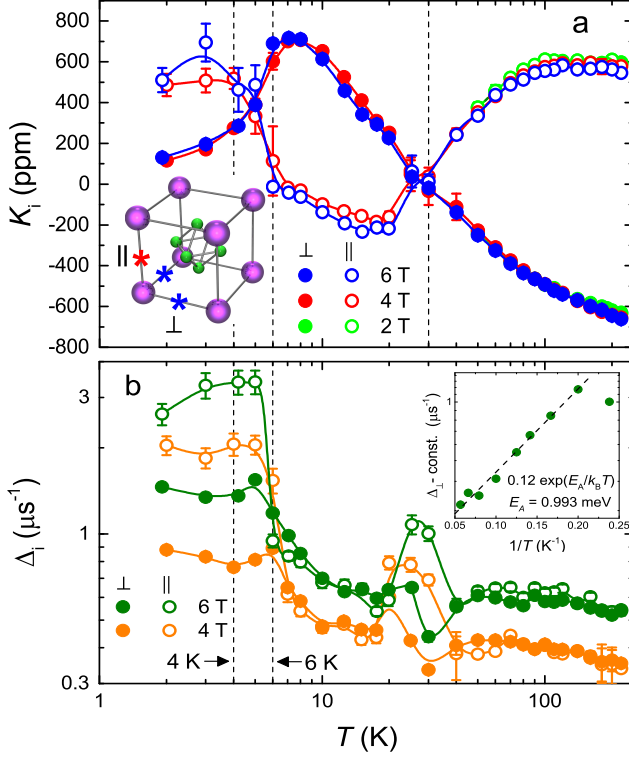


FIG. 3. Temperature dependence of **a** the μ^+ -Knight shifts, and **b** the TF- μ SR relaxation rates at magnetic fields of 4 T and 6 T applied parallel to the c -axis. Data at $H=2$ T is also shown in **a** for $T \geq 50$ K, below which the different components of the TF- μ SR signal are not clearly resolved. The error bars represent the uncertainties in the parameters ν_i and Δ_i from the fits in the time domain. The inset in **a** shows the two magnetically-inequivalent muon sites on the vertical (\parallel) and horizontal edges (\perp) of the Sm-ion cubic sublattice. The inset in **b** shows a semi-log plot of Δ_{\perp} (minus a constant) versus $1/T$, for $4.2 \leq T \leq 17.6$ K. The straight dashed line is a fit of the data for $T \geq 5$ K to a thermally-activated function.

Also, $\nu_i = (\gamma_{\mu}/2\pi)B_{\mu,i}$ and $\Delta_i^2 = \gamma_{\mu}^2 \langle \mathbf{B}_{\mu,i}^2 \rangle$, where $\gamma_{\mu}/2\pi = 135.54$ MHz/T and $B_{\mu,i}$ and $\langle \mathbf{B}_{\mu,i}^2 \rangle$ are the local magnetic field and width of the field distribution at the μ^+ sites ($i = \perp, \parallel$, and Ag), respectively. The initial phase of the muon spin polarization is denoted by ϕ . As the temperature is lowered ν_{\perp} (ν_{\parallel}) increases (decreases), and below $T \sim 30$ K the \perp (\parallel) peak in the Fourier transform broadens and moves to the far right (left). Even so, the two sample components are observed to maintain a population ratio of 2:1 down to 1.9 K. We note that the 6 T applied magnetic field is far below the field of 80-90 T required to close the insulating gap.⁴⁰

The relative frequency shift is defined as $K_{\mu,i} = (\nu_i - \nu_0)/\nu_0$, where $\nu_0 = (\gamma_{\mu}/2\pi)H$. After correcting for the demagnetization and Lorentz fields, the μ^+ -Knight shift

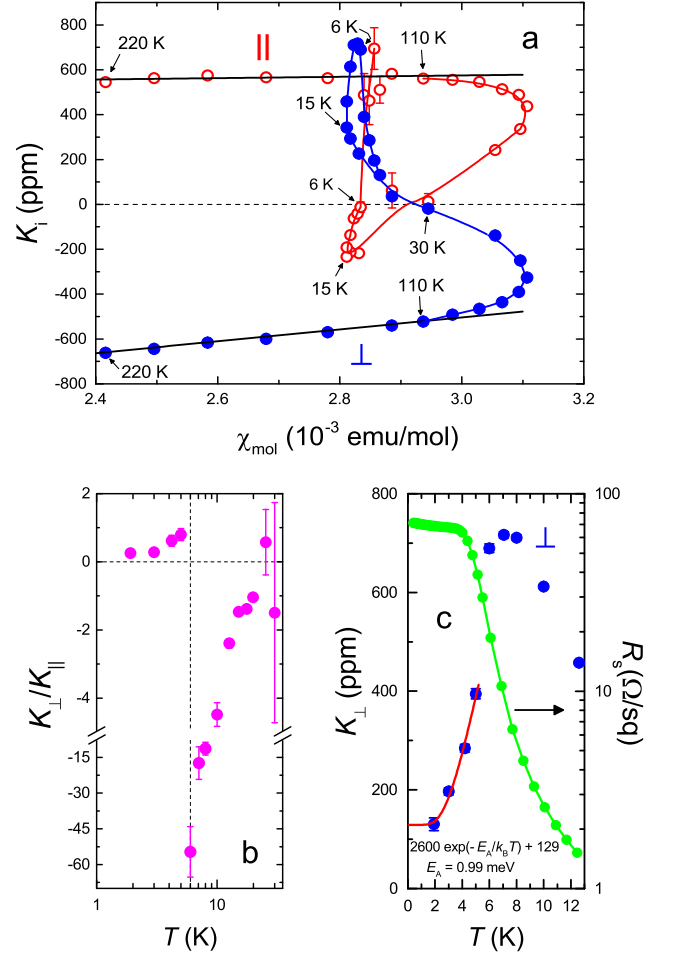


FIG. 4. **a** Knight shift at the two magnetically-inequivalent μ^+ sites versus χ_{mol} at $H=6$ T. Temperature is an implicit parameter. The straight black lines are fits to equations (4a) and (4b). Temperature dependence of **b** the ratio K_{\perp}/K_{\parallel} below 30 K, and **c** K_{\perp} and the electrical sheet resistance below 13 K. The red curve is a fit of the K_{\perp} data for $T \leq 5$ K to a thermally-activated Arrhenius equation, assuming an activation energy $E_A = 0.99$ meV.

at the magnetically inequivalent muon sites is

$$K_{\perp}(T) = (A_c^{\perp} - \frac{1}{2}A_{\text{dip}})\chi_{4f}(T) + K_0^{\perp}, \quad (4a)$$

$$K_{\parallel}(T) = (A_c^{\parallel} + A_{\text{dip}})\chi_{4f}(T) + K_0^{\parallel}, \quad (4b)$$

where A_c^i and A_{dip} are the contact hyperfine and dipolar coupling constants, $\chi_{4f} = \chi_{\text{mol}} - \chi_0$ is the local $4f$ magnetic susceptibility, and χ_0 and K_0^i are the Pauli paramagnetic susceptibility and corresponding Knight shifts, respectively.

Figure 3 shows the temperature dependence of the Knight shifts K_i and TF relaxation rates Δ_i . In contrast to χ_{mol} , the Knight shifts below 17 K do not exhibit an appreciable field dependence. We attribute the jump (dip) in Δ_{\perp} (Δ_{\parallel}) between 20 and 40 K to fit pa-

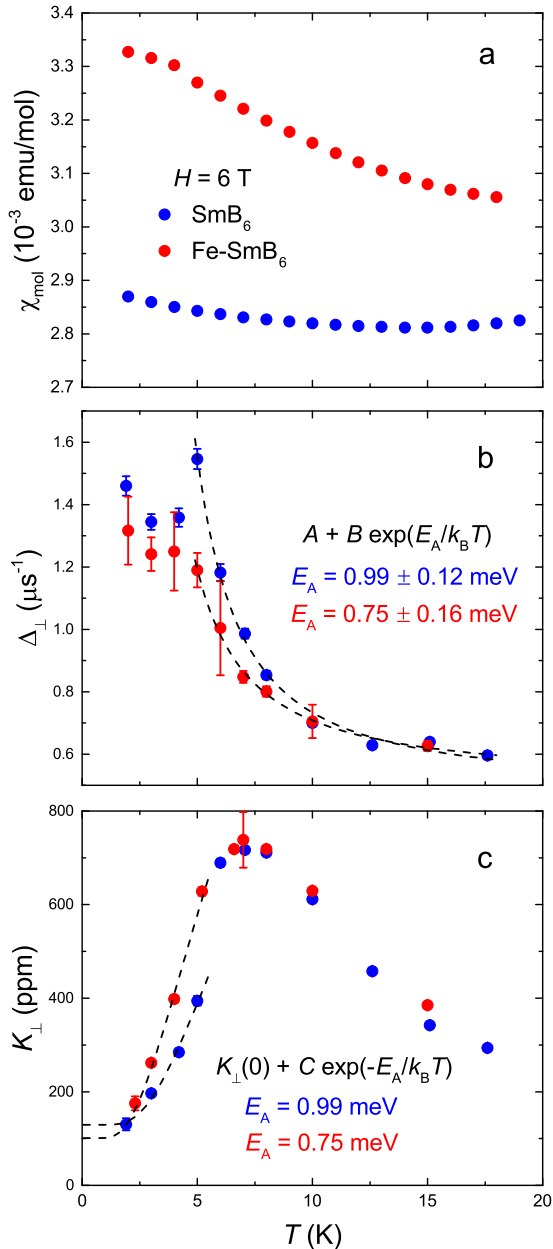


FIG. 5. Temperature dependences of the low-temperature **a** bulk magnetic susceptibility, **b** TF- μ SR relaxation rate Δ_{\perp} , and **c** Knight shift K_{\perp} in pure and 0.5 % Fe-doped SmB₆ for $H = 6$ T. The dashed curves in **b** are fits of the Δ_{\perp} data above 5 K to a thermally-activated function $A + B \exp(E_A/k_B T)$. The dashed curves in **c** are fits of the K_{\perp} data at $T \leq 5$ K to a thermally-activated Arrhenius equation $K_{\perp}(0) + C \exp(-E_A/k_B T)$ assuming the values of E_A from the fits in **b**.

rameters playing off against each other, as $\nu_{\perp} \sim \nu_{\parallel}$ in this temperature range.

Figure 4a shows the Knight shift data plotted versus χ_{mol} with temperature as an implicit parameter (a so-called Clogston-Jaccarino plot). We find that a plot of $K_{\perp} - K_{\parallel}$ versus χ_{mol} above 110 K (not shown) is linear as expected from equations (4a) and (4b), but has a slope and intercept incompatible with A_c and K_0 being isotropic. Using the calculated value $A_{\text{dip}} = 0.395$ T/ μ_B for the μ^+ site, linear fits of the Knight shifts in SmB₆ above 110 K to equations (4a) and (4b) yield $A_c^{\perp} = 0.346$ T/ μ_B and $A_c^{\parallel} = -0.378$ T/ μ_B . This anisotropy can be explained by the influence of the Sm $4f^5$ -shell electric quadrupole moment⁴¹ on the conduction electron spin polarization at the μ^+ site, which has been observed in other compounds with non-spherical f -electron distributions.⁴²

Below 110 K, the K_i versus χ_{mol} plots deviate from linearity (see Fig. 4a). Point-contact spectroscopy⁴³ and ARPES⁴⁴ measurements on SmB₆ show the hybridization gap develops over a fairly wide temperature range of $30 \text{ K} \lesssim T \lesssim 110 \text{ K}$. This results in a loss of scaling between K_i and χ_{mol} , due to a gradual reduction of both the Pauli susceptibility ($\propto K_0^i$) and the electronic spin density at the μ^+ sites ($\propto A_c^i$). Near 30 K, the simultaneous vanishing of K_{\perp} and K_{\parallel} implies $K_0^i = 0$ and $\chi_{4f} = 0$ in equations (4a) and (4b).

Below $T \sim 25$ K a μ^+ -Knight shift reappears, which does not linearly scale with χ_{mol} (Fig. 4a) and is accompanied by an increase in the TF relaxation rates with decreasing T (Fig. 3b).

DISCUSSION

The μ^+ -Knight shift below 25 K is a property of the insulating bulk. In insulators and semiconductors the μ^+ sometimes forms a bound state with an electron, known as a *muonium* atom (Mu).³⁸ The signature of Mu in high TF is a pair of frequencies separated by the Mu hyperfine splitting and centered on the precession frequency of the free μ^+ in the applied field — the latter being close to the μ^+ precession frequency in the Ag backing plate. This is clearly not observed in Fig. 2. Consequently, the μ^+ -Knight shift must still be induced by the Sm- $4f$ moments.

The lack of scaling of K_i with the bulk magnetic susceptibility χ_{mol} below 25 K could potentially arise from the charged muon significantly altering the Sm³⁺ crystal electric field (CEF) level scheme and hence χ_{4f} . A significant influence of the μ^+ on the local magnetic susceptibility has been identified in a few Pr³⁺-ion systems.^{45,46} The CEF level scheme of Sm³⁺ ($4f^5$) in SmB₆ is similar to Ce³⁺ ($4f^1$) in CeB₆. In both cases the spin-orbit interaction splits the $4f$ states into $J = 5/2$ and $J = 7/2$ multiplets. The $J = 5/2$ multiplet is further split in the cubic crystalline field into a Γ_7 doublet, and a ground-state Γ_8 quartet that has magnetic and quadrupolar moments. The energy difference between the Γ_8 quartet and excited Γ_7 doublet is about 15 meV in SmB₆,⁴⁷ and 46 meV in CeB₆,⁴⁸ which in both compounds exceeds the

Kondo energy scale (temperature). Thus, only modifications of the Zeeman split Γ_8 quartet are relevant in the low T regime. In CeB₆, which does not develop a Kondo insulating gap, K_i linearly scales with χ_{mol} above 10 K. Hence it is unlikely that the μ^+ induces the Knight shift observed in SmB₆ below 20 K. We note that the loss of scaling between K_i and χ_{mol} in CeB₆ below 10 K is due to the development of antiferroquadrupolar ordering,⁴⁹ which does not occur in SmB₆.

According to equations (4a) and (4b), there must be a new contact hyperfine field \mathbf{B}_c to cause the sign change in the values of K_\perp and K_\parallel below 25 K. As mentioned earlier, in an insulating state this may result from the μ^+ bonding to an ion that is covalently bonded to a localized magnetic electron. A *super-transferred hyperfine field* at the μ^+ site through a Sm-B- μ^+ connection could arise from field-induced moments at the B sites. In CeB₆, field-induced magnetic moments inside or around the B₆ octahedron have been ruled out by polarized neutron diffraction,⁵⁰ which is presumably also the case in SmB₆. Moreover, the formation of a B- μ^+ bond is incompatible with the μ^+ site, which is $\sim 2 \text{ \AA}$ from the nearest B atom.

The alternative possibility in an insulating state is that \mathbf{B}_c originates from direct overlap of the μ^+ with the wavefunction of the localized magnetic electrons. While the Sm-4*f* orbitals are highly localized, the 5*d* orbitals of the nearest-neighbor Sm ions partially overlap the μ^+ site. In a spin exciton the spin polarization of the bound 5*d* electron is coherently coupled to the localized 4*f* electrons, and a contact hyperfine field may result from an exchange interaction between the μ^+ and the extended magnetic 5*d* electrons.

The temperature dependence of the TF- μ SR relaxation rate (Fig. 3b) provides evidence for a low-energy spin exciton. The marked increase of Δ_\perp and Δ_\parallel below 20 K corresponds to an increase in the width of the local field distribution, indicative of a gradual slowing down of magnetic fluctuations. As shown in the inset of Fig. 3b, the $H = 6 \text{ T}$ data for Δ_\perp above 5 K can be fit with a thermally-activated law: $\Delta_\perp = A + B \exp(E_A/k_B T)$, yielding $A = 0.35 \pm 0.07 \text{ } \mu\text{s}^{-1}$, $B = 0.12 \pm 0.04 \text{ } \mu\text{s}^{-1}$, and $E_A = 0.99 \pm 0.12 \text{ meV}$. A temperature-independent contribution comes from the nuclear dipole moments and the spatial inhomogeneity of the applied magnetic field. The thermally-activated decrease of Δ_\perp is consistent with a rising fluctuation rate ($1/\tau$), where $1/\tau \propto \exp(-E_A/k_B T)$. Spin excitons create fluctuating regions of AFM correlations extending over a few unit cells, which modify the local fields sensed by the μ^+ . The increase in Δ_i is explained by AFM amplitude fluctuations perpendicular to \mathbf{H} , producing a small temporary canted moment. This is presumably of order H/J_{RKKY} , where J_{RKKY} is the virtual RKKY-like magnetic exchange interaction between the 4*f* moments in the theory of Riseborough.^{26,27} The nearly constant difference between Δ_i at 6 T and 4 T above 6 K is primarily caused by a difference in the inhomogeneity of the applied field.

Below 5-6 K, however, Δ_i saturates and exhibits an intrinsic increase with H . The saturation indicates that the average fluctuation period of the spin excitons (τ) has become large with respect to the muon time window, such that Δ_i is no longer significantly affected by fluctuations. The corresponding field-dependence of Δ_i below 5-6 K reflects an inhomogeneous broadening of the local field distribution.

Figure 4b shows a strong temperature dependence of K_\perp/K_\parallel at $6 \lesssim T \lesssim 20 \text{ K}$, which with $K_0^i = 0$ reflects the behavior of $(A_c^\perp - A_{\text{dip}}^\perp/2)/(A_c^\parallel + A_{\text{dip}}^\parallel)$. Changes in the lattice parameter^{20,51,52} below 20 K are too small to cause an appreciable change in A_{dip} . The remaining possibility is that A_c^\perp and A_c^\parallel change with decreasing temperature. The anisotropy of A_c above 110 K indicates coupling of the non-spherical 4*f*-electron distribution to the field-induced Sm magnetic moments. Hence, the strong temperature dependence of A_c^\perp and A_c^\parallel below 20 K is likely due a rotation of the 4*f*-electron distribution with the canted moment induced by AFM fluctuations. We note that the values of A_c^i are dependent on the overlap integral of the non-spherical 4*f*-electron distribution and the 5*d* electrons with wavefunctions that overlap the μ^+ site. Below 6 K there is an abrupt increase in K_\perp/K_\parallel to a value comparable to that at 25 K. This suggests that the 4*f*-electron distribution returns to being more closely aligned with the applied field.

As shown in Fig. 3a, there is an abrupt decrease (increase) in K_\perp (K_\parallel) below 5-6 K. According to equations (4a) and (4b), these simultaneous behaviors cannot be explained by a rapid change in $\chi_{4f}(T)$. Instead these behaviors appear to reflect the temperature dependence of K_\perp/K_\parallel (and hence A_c^\perp and A_c^\parallel) that is apparent at $T \leq 5 \text{ K}$ in Fig. 4b. As shown in Fig. 4c, the temperature dependence of K_\perp for $T \leq 5 \text{ K}$ is well fit with a thermally-activated Arrhenius equation: $K_\perp(T) = K_\perp(0) + C \exp(-E_A/k_B T)$ that assumes the same value $E_A = 0.99 \text{ meV}$ obtained from the fit of the temperature dependence of Δ_\perp .

The dynamic relaxation rate λ_{ZF} observed by zero-field (ZF) μ SR develops below 20-25 K,²² exhibits a short anomalous peak near 4 K and subsequently saturates. Our findings here suggest that the saturation is due to the freezing out of a bulk spin exciton of much lower energy than that observed by INS, giving way to AFM quantum spin fluctuations. We note that the peak in $\lambda_{\text{ZF}}(T)$ near 4 K vanishes with the addition of a 0.5 % Fe impurity.²³ This is likely due to the predicted adverse effect of impurities on a fully developed spin exciton.²⁷ We have carried out similar TF- μ SR measurements on the 0.5 % Fe-doped sample. Figure 5 shows a comparison of the low-temperature results with those for the pure compound. While the bulk magnetic susceptibility is significantly modified by the Fe impurities, the changes to the temperature dependences of Δ_\perp and K_\perp are more subtle. A fit of the Δ_\perp versus T data for the Fe-doped sample above 5 K to the thermally-activated law described ear-

lier yields $E_A = 0.75 \pm 0.16$ meV. The smaller activation energy compared to pure SmB_6 is consistent with the expected impurity-induced broadening and decrease of the binding energy of the spin exciton.²⁷

As shown in Fig. 4c, the saturation of the electrical sheet resistance R_s occurs below 4 K, where K_\perp is greatly reduced. Thus the resistivity plateau apparently occurs when spin exciton scattering of the metallic surface states becomes negligible. Our findings support the theoretical prediction of a low-energy spin exciton ($\lesssim 1$ meV) in SmB_6 , which has been argued to account for certain low-temperature thermodynamic and transport anomalies.³³

METHODS

Samples and experimental technique

The growth and characterization of the crystals were previously reported.²³ The high TF μ^+ -Knight shift measurements were performed on a 5×5 mm² mosaic of single crystals aligned with the c -axis parallel to the applied field and mounted on a pure Ag backing plate. The measurements utilized a He-gas flow cryostat and the so-called “NuTime” spectrometer at TRIUMF in Vancouver, Canada. All of the high TF- μ SR measurements were recorded with the initial muon spin polarization $\mathbf{P}(0)$ perpendicular to the external magnetic field \mathbf{H} , which was applied parallel to the muon beam momentum. Figure S1 shows a schematic of a custom sample holder designed for the μ^+ -Knight shift measurements.

The value of the muon spin precession frequency in the applied magnetic field H alone, $\nu_0 = (\gamma_\mu/2\pi)H$, was accurately determined by first simultaneously recording the TF- μ SR signal

in a 99.998 % pure Ag mask located upstream of the sample. To correct for the difference in the external field at the Ag mask and sample locations, TF- μ SR measurements were also simultaneously performed on the Ag mask with Ag in place of SmB_6 at the sample location.

Data availability

All relevant data are available upon request from the corresponding authors.

ACKNOWLEDGEMENTS

This work was performed at TRIUMF, the University of Maryland (UofM) and Simon Fraser University (SFU). J.E.S. acknowledges support from NSERC of Canada. J.P. acknowledges support from AFOSR through Grant No. FA9550-14-1-0332 and the Gordon and Betty Moore Foundation’s EPiQS Initiative through Grant No. GBMF4419. The authors wish to thank E. Mun, J. S. Dodge and P. S. Riseborough for informative discussions.

AUTHOR CONTRIBUTIONS

S.R.S., X.F.W., J.P., grew and characterized the sample. K.A. performed the bulk magnetic susceptibility measurements. K.A., A.P., S.R.D., A.C.Y.F., M.P., S.R.S., and J.E.S. performed the high TF- μ SR measurements at TRIUMF. K.A. and J.E.S. carried out the data analysis. K.A. and J.E.S. wrote the manuscript with input from all co-authors.

ADDITIONAL INFORMATION

Supplementary information accompanies the paper.

Competing interests: The authors declare no competing interests.

-
- ¹ Hasan, M. Z. & Kane, C. L. Colloquium: Topological insulators. *Rev. Mod. Phys.* **82** 3045-3067 (2010).
 - ² Ando, Y. Topological insulator materials. *J. Phys. Soc. Jpn.* **82**, 102001 (2013).
 - ³ Dzero, M., Xia, J., Galitski, V., & Coleman, P. Topological Kondo insulators. *Annu. Rev. Condens. Matter Phys.* **7**, 249-280 (2016).
 - ⁴ Kim, D. J., Thomas, S., Grant, T., Botimer, J., Fisk, Z. & Xia, J. Surface Hall effect and nonlocal transport in SmB_6 : Evidence for surface conduction. *Scientific Reports* **3**, 3150 (2013).
 - ⁵ Wolgast, S. *et al.* Low-temperature surface conduction in the Kondo insulator SmB_6 . *Phys. Rev. B* **88**, 180405(R) (2013).
 - ⁶ Kim, D. J., Xian, J. & Fisk, Z. Topological surface state in the Kondo insulator samarium hexaboride. *Nat. Mater.* **13**, 466-470 (2014).
 - ⁷ Jiang, J. *et al.* Observation of possible topological in-gap surface states in the Kondo insulator SmB_6 by photoemission. *Nat. Commun.* **4**, 3010 (2013).
 - ⁸ Xu, N. *et al.* Surface and bulk electronic structure of the strongly correlated system SmB_6 and implications for a topological Kondo insulator. *Phys. Rev. B* **88**, 121102(R) (2013).
 - ⁹ Neupane, M. *et al.* Surface electronic structure of the topological Kondo-insulator candidate correlated electron system SmB_6 . *Nat. Commun.* **4**, 2991 (2013).
 - ¹⁰ Frantzeskakis, E. *et al.* Kondo hybridization and the origin of metallic states at the (001) surface of SmB_6 . *Phys. Rev. X* **3**, 041024 (2013).
 - ¹¹ Xu, N. *et al.* Direct observation of the spin texture in SmB_6 as evidence of the topological Kondo insulator. *Nat. Commun.* **5**, 4566 (2014).
 - ¹² Hlawenka, P. *et al.* Samarium hexaboride is a trivial surface conductor. *Nat. Commun.* **9**, 517 (2018).
 - ¹³ Wakeham, N. *et al.* Low-temperature conducting state in two candidate topological Kondo insulators: SmB_6 and $\text{Ce}_3\text{Bi}_4\text{Pt}_3$. *Phys. Rev. B* **94**, 035127 (2016).
 - ¹⁴ Laurita, N. J. *et al.* Anomalous three-dimensional bulk ac conduction within the Kondo gap of SmB_6 single crystals. *Phys. Rev. B* **94**, 165154 (2016).
 - ¹⁵ Li, G. *et al.* Two-dimensional Fermi surfaces in Kondo insulator SmB_6 . *Science* **346**, 1208-1212 (2014).
 - ¹⁶ Tan, B. S. *et al.* Unconventional Fermi surface in an insulating state. *Science* **349**, 287-290 (2015).
 - ¹⁷ Baskaran, G. Majorana Fermi sea in insulating SmB_6 : A proposal and a theory of quantum oscillations in Kondo insulators. Preprint at <https://arxiv.org/abs/1507.03477> (2015).
 - ¹⁸ Erten, O., Chang, P. -Y., Coleman, P. & Tsvelik, A. M. Skyrme Insulators: Insulators at the brink of superconductivity. *Phys. Rev. Lett.* **119**, 057603 (2017).
 - ¹⁹ Chowdhury, D., Sodemann, I. & Senthil, T. Mixed-valence insulators with neutral Fermi-surfaces. Preprint at <https://arxiv.org/abs/1706.00418> (2017).
 - ²⁰ Tarascon, J. M. *et al.* Temperature dependence of the samarium oxidation state in SmB_6 and $\text{Sm}_{1-x}\text{La}_x\text{B}_6$. *J. Phys. France* **41**, 1141 (1980).

- ²¹ Mizumaki, M., Tsutsui, S. & Iga, F. Temperature dependence of Sm valence in SmB₆ studied by X-ray absorption spectroscopy. *J. Phys.: Conf. Ser.* **176**, 012034 (2009).
- ²² Biswas, P. K. *et al.* Low-temperature magnetic fluctuations in the Kondo insulator SmB₆. *Phys. Rev. B* **89**, 161107 (2014).
- ²³ Akintola, K. *et al.* Quantum spin fluctuations in the bulk insulating state of pure and Fe-doped SmB₆. *Phys. Rev. B* **95**, 245107 (2017).
- ²⁴ Caldwell, T. *et al.* High-field suppression of in-gap states in the Kondo insulator SmB₆. *Phys. Rev. B* **75**, 075106 (2007).
- ²⁵ Biswas, P. K. *et al.* Suppression of magnetic excitations near the surface of the topological Kondo insulator SmB₆. *Phys. Rev. B* **95**, 020410(R) (2017).
- ²⁶ Riseborough, P. S. Magnetic bound states in SmB₆. *Ann. Phys.* **9**, 813-820 (2000).
- ²⁷ Riseborough, P. S. Collapse of the coherence gap in Kondo semiconductors. *Phys. Rev. B* **68**, 235213 (2003).
- ²⁸ Alekseev, P. A. *et al.* Magnetic excitation spectrum of mixed-valence SmB₆ studied by neutron scattering on a single crystal. *J. Phys.: Condens. Matter* **7**, 289-305 (1995).
- ²⁹ Fuhrman, W. T. *et al.* Interaction driven subgap spin exciton in the Kondo insulator SmB₆. *Phys. Rev. Lett.* **114**, 036401 (2015).
- ³⁰ Kapilevich, G. A. *et al.* Incomplete protection of the surface Weyl cones of the Kondo insulator SmB₆: Spin exciton scattering. *Phys. Rev. B* **92**, 085133 (2015).
- ³¹ Arab, A. *et al.* Effects of spin excitons on the surface states of SmB₆: A photoemission study. *Phys. Rev. B* **94**, 235125 (2016).
- ³² Park, W. K. *et al.* Topological surface states interacting with bulk excitations in the Kondo insulator SmB₆ revealed via planar tunneling spectroscopy. *PNAS* **113**, 6599-6604 (2016).
- ³³ Knolle, J. & Cooper, N. R. Excitons in topological Kondo insulators: Theory of thermodynamic and transport anomalies in SmB₆. *Phys. Rev. Lett.* **118**, 096604 (2017).
- ³⁴ Fuhrman W. T. *et al.* Screened moments in a Kondo insulator. Preprint at <https://arxiv.org/abs/1707.03834> (2017).
- ³⁵ Orendáč, M. *et al.* Isosbestic points in doped SmB₆ as features of universality and property tuning. *Phys. Rev. B* **96**, 115101 (2017).
- ³⁶ Roman, J. *et al.* Low temperature magnetic properties of samarium hexaboride. *Czech. J. Phys.* **46**, 1983 (1996).
- ³⁷ Gabáni, S. *et al.* Magnetic properties of SmB₆ and Sm_{1-x}La_xB₆ solid solutions. *Czech. J. Phys.* **52**, A225-A228 (2002).
- ³⁸ Schenck, A. Muon Spin Rotation Spectroscopy: *Principles and Applications in Solid State Physics*, Adam Hilger Ltd, England, 1985.
- ³⁹ Schenck, A., Gygax, F. N. & Kunii, S. Field-induced magnetization distribution and antiferroquadrupolar order in CeB₆. *Phys. Rev. Lett.* **89**, 037201 (2002).
- ⁴⁰ Cooley, J. C. *et al.* High field gap closure in the Kondo insulator SmB₆. *J. Supercond.* **12**, 171 (1999).
- ⁴¹ Delyagin, N. N. & Erzinkyan, A. L. The impact of quadrupole moment of 4f shell on the hyperfine interactions anisotropy in RAl₂ (R=Sm, Tb) intermetallic compounds. *Solid State Commun.* **230**, 16-19 (2016).
- ⁴² Schenck, A., Gygax, F. N., Andreica, D. & Onuki, Y. J. Interplay of quadrupolar order, Ce 4f spin dynamics and RKKY induced conduction electron spin polarization in CeAg. *Phys.: Condens. Matter* **15**, 8599-8617 (2003).
- ⁴³ Zhang, X. *et al.* Hybridization, inter-ion correlation, and surface states in the Kondo insulator SmB₆. *Phys. Rev. X* **3**, 011011 (2013).
- ⁴⁴ Xu, N *et al.* Exotic Kondo crossover in a wide temperature region in the topological Kondo insulator SmB₆ revealed by high-resolution ARPES. *Phys. Rev. B* **90**, 085148 (2014).
- ⁴⁵ Feyerherm, R. *et al.* Crystal electric field next to a hydrogen-like interstitial- μ^+ in PrNi₅. *Phys. B* **99**, 3 (1995).
- ⁴⁶ Tashma, T. *et al.* Electronic changes induced by μ^+ in PrIn₃: Muon-spin-rotation observation and crystalline-electric-field model calculation. *Phys. Rev. B* **56**, 9397 (1997).
- ⁴⁷ Sundermann, M. *et al.* 4f Crystal field ground state of the strongly correlated topological insulator SmB₆. *Phys. Rev. Lett.* **120**, 016402 (2018).
- ⁴⁸ Sundermann, M. *et al.* The quartet ground state in CeB₆: An inelastic x-ray scattering study. *Europhys. Lett.* **117**, 17003 (2017).
- ⁴⁹ Schenck, A., Gygax, F. N., Solt, G., Zaharko, O. & Kunii, S. Temperature and field dependence of the order parameter in the antiferroquadrupolar phase of CeB₆ from μ^+ Knight Shift measurements. *Phys. Rev. Lett.* **93**, 257601 (2004).
- ⁵⁰ Givord, F., Boucherle, J. -X., Burlet, P., Gillon, B. & Kunii, S. Non-anomalous magnetization density distribution in CeB₆. *J. Phys. Condens. Matter* **15**, 3095 (2003).
- ⁵¹ Sirota, N. N., Novikov, V. V., Vinokurov, V. A. & Paderno, Yu. B. Temperature dependence of the heat capacity and lattice constant of lanthanum and samarium hexaborides. *Phys. Solid State* **40**, 1856 (1998).
- ⁵² Mandrus, D. *et al.* Low-temperature thermal expansion of SmB₆: Evidence for a single energy scale in the thermodynamics of Kondo insulators. *Phys. Rev. B* **49**, 16809 (2002).